

ILMATIETEEN LAITOS
METEOROLOGISKA INSTITUTET
FINNISH METEOROLOGICAL INSTITUTE

PLUMO

Parameterized dataset of representative SMR dispersion scenarios

Deliverable:	D1.1.1
Work Package:	WP1
Authors:	Antti Hellsten, Mikko Auvinen, Mari Kauhaniemi Jukka-Pekka Keskinen, Mia Aarnio
Authors*:	Mikko Ilvonen, Jenna Järvenpää
Authors †:	Benjamin Grigoriadis
Organisations:	Ilmatieteen laitos, VTT *, Fortum Power and Heat Oy †
Date:	September 11, 2026
Reviewed by:	Reko Rantamäki and Juha-Pekka Jurvanen, Fortum Power and Heat Oy

Confidentiality: Public

Contents

1 Executive Summary **2**

2 Introduction **2**

3 Materials and methods **2**
3.1 Materials . . . 2
3.2 Set of urban canopy parameters and computational methods . . . 3
3.3 Set of plant canopy parameters . . . 6

4 Suite of selected built environments **6**
4.1 Real built environments . . . 8
4.1.1 R1 Helsinki Vuosaari . . . 8
4.1.2 R2 Kuopio/Siilinjärvi Sorsasalo-Vuorela . . . 9
4.1.3 R3 Helsinki Kallio-Hakaniemi-Kruununhaka . . . 9
4.1.4 R4 Turku Kaerla . . . 9
4.2 Generic built environments . . . 10
4.2.1 G11 Generic homogenized Vuosaari-port-like warehouse area variant 1 . . . 10
4.2.2 G12 Generic homogenized Vuosaari-port-like warehouse area variant 2 . . . 10
4.2.3 G13 Generic homogenized variant of Vuosaari residential area . . . 10
4.2.4 G21 Generic homogenized variant of Vuorela, Siilinjärvi, residential area . . . 10
4.2.5 G22 Generic homogenized variant of Vuorela, Siilinjärvi, warehouse-area . . . 11
4.2.6 G31 Generic homogenized variant of Kallio, Helsinki . . . 11
4.2.7 G32 Generic homogenized variant of Kruununhaka/Kaisaniemi, Helsinki . . . 11
4.2.8 G41 homogenized variant of Kaerla, Turku, detached-house area . . . 11
4.2.9 G42 homogenized variant of Kaerla, Turku, apartment-building area . . . 12
4.3 Summary of the parameters . . . 12

5 Selected meteorological conditions **13**

6 Next steps **14**

7 References **15**

A Building- and tree-height raster plots **16**
A.1 Case R1 Helsinki Vuosaari . . . 16
A.2 Case R2 Kuopio/Siilinjärvi Sorsasalo-Vuorela . . . 17
A.3 Case R3 Helsinki Kallio-Hakaniemi-Kruununhaka . . . 18
A.4 Case R4 Turku Kaerla . . . 19
A.5 Case G11 Generic homogenized Vuosaari-port-like warehouse area variant 1 . . . 20
A.6 Case G12 Generic homogenized Vuosaari-port-like warehouse area variant 2 . . . 20
A.7 Case G13 Generic homogenized variant of Vuosaari residential area . . . 21
A.8 Case G21 Generic homogenized variant of Vuorela, Siilinjärvi, residential area . . . 22
A.9 Case G22 Generic homogenized variant of Vuorela, Siilinjärvi, warehouse area . . . 23
A.10 Case G31 Generic homogenized variant of Kallio, Helsinki . . . 24
A.11 Case G32 Generic homogenized variant of Kruununhaka/Kaisaniemi, Helsinki . . . 25
A.12 Case G41 Generic homogenized variant of Kaerla, Turku, detached-house area . . . 26
A.13 Case G42 Generic homogenized variant of Kaerla, Turku, apartment-building area 27

1 Executive Summary

This deliverable report documents the first phase of the PLUMO (SAFER2028) project, which focuses on the use of high-resolution Large-Eddy Simulation (LES) to study near-source dispersion of airborne radioactive releases from Small Modular Reactor (SMR) accident scenarios in built environments. The overall objective of the project is to improve the predictive capacity of existing low-cost dispersion models by parametrizing both the meteorological conditions via meteorological parameters (MEPs) and the roughness characteristics of the surrounding landscape via Urban Canopy and Plant Canopy Parameters (UCPs and PCPs respectively). This report introduces the relevant set of UCPs, PCPs, and MEPs, provides their definitions and presents a suite of built environments to be modelled by LES and used for enabling improvements of the low-cost dispersion models through machine learning techniques.

2 Introduction

Recent changes in the energy and policy landscape have renewed interest in nuclear power, particularly Small Modular Reactors (SMRs), which are expected to offer flexible, low-carbon energy production with improved safety and reduced costs. In Finland, this development is supported by extensive experience in nuclear energy and established waste management practices. Traditional atmospheric dispersion modelling for nuclear accidents has focused on distances beyond approximately 1 km, reflecting the large site areas of conventional nuclear power plants and emergency planning practices. However, SMRs are likely to be deployed closer to populated or industrial areas, shifting the focus to near-field dispersion and more complex built environments. Urban structures significantly influence dispersion through increased surface roughness, enhanced turbulence, and channeling effects. These conditions challenge the applicability of simple dispersion models, emphasizing the need for improved parametrizations and high-resolution modelling approaches.

This deliverable report D1.1.1 documents the first phase of the PLUMO (SAFER2028) project, which focuses on the use of high-resolution Large-Eddy Simulation (LES) to study near-source dispersion of airborne radioactive releases from Small Modular Reactor (SMR) accident scenarios in built environments. The overall objective of the project is to improve the predictive capacity of existing low-cost dispersion models by parametrizing both the meteorological conditions via meteorological parameters (MEPs) and the roughness characteristics of the surrounding landscape via Urban Canopy and Plant Canopy Parameters (UCPs and PCPs respectively). To this end, LES-modelled dispersion outcomes will be systematically catalogued together with their corresponding parameter sets, enabling quantitative comparison with low-cost models and supporting their improvement through machine learning techniques. In this first phase, the project concentrates on defining a sufficiently representative set of UCPs and PCPs that capture the key morphological features governing near-field dispersion in built environments.

This report introduces the relevant set of UCPs, PCPs, and MEPs, provides their definitions and presents a suite of built environments relevant to this project.

3 Materials and methods

3.1 Materials

In this report, raster-based elevation datasets of buildings and vegetation are used to characterize the selected built environments. A raster format is required because the PALM LES model represents orography, building topography, and vegetation canopy height on gridded input fields [Maronga et al., 2015, 2020].

The terrain elevation data is provided by National Land Survey [2026a]. For Helsinki (Vuosaari) and Kuopio/Siilinjärvi (Sorsasalo–Vuorela), the datasets are derived from the most recent open-access Canopy Height Model (CHM) provided by the Finnish Forest Centre [2026], together with building outlines from the National Land Survey's Topographic Database [National Land Survey, 2026b]. The CHM represents the height difference between the vegetation canopy and ground surface, but also includes buildings as elevated features; therefore, 2D building data are used to separate buildings from vegetation.

The dataset for Helsinki (Kallio–Hakaniemi–Kruununhaka) is based on open-access LiDAR data provided by the City City of Helsinki [2015] and processed for LES applications in Auvinen et al. [2020]. The Turku (Kaerla) dataset is derived from 3D laser scanning data provided by the City of Turku [2021] (2021).

3.2 Set of urban canopy parameters and computational methods

Effects of urban and built canopies on turbulent flow are typically parameterized using bulk metrics such as mean building height $\overline{h_b}$, its standard deviation σ_{h_b}, plan-area fraction $\lambda_{pb} = A_{pb}/A_T$, and frontal-area fraction $\lambda_{fb} = A_{fb}/A_T$, where A_{pb} is the building plan area, A_{fb} the frontal area, and A_T the total domain area [Oke et al., 2017]. While these parameters can adequately describe idealized urban configurations, real urban and peri-urban environments are more complex, heterogeneous, and often anisotropic. A fully general finite parameter set is therefore not attainable; instead, the objective is to define a practically useful parameterization that captures the dominant geometric controls on near-field dispersion.

The frontal-area fraction λ_{fb} is, in principle, wind-direction dependent. For sufficiently large and morphologically diverse areas, this dependence is expected to be weaker than for regular, idealized geometries. However, the raster representation of building topography introduces directional bias when estimating λ_{fb} for arbitrary directions. For this reason, λ_{fb} is computed only along the x- and y-axes. As shown in Sec. 4, the resulting values are very similar for all selected cases, indicating weak directional dependence.

An important feature of built canopies is their tendency to induce wind channeling. When major street canyons or other elongated open areas are aligned with the mean wind direction θ, they can strongly control the local flow within and immediately above the canopy. In addition, such uninterrupted canyons modify the structure of coherent turbulent motions within the roughness sublayer (RSL), i.e. within approximately 4–5 canopy heights [Inagaki et al., 2012]. These effects are not captured by the standard set of bulk morphological parameters.

To quantify channeling, Lu et al. [2023] introduced an alignedness metric γ that characterizes the presence and dominance of elongated canyons aligned with the mean wind direction. Here, we adopt and generalize this approach. The computational procedure is based on traversing the domain with a set of parallel lines oriented along a prescribed mean wind direction. The line spacing is equal to the grid resolution. For each line, uninterrupted segments between solid obstacles (buildings or other structures) are identified and their lengths recorded, while segments within buildings are excluded. Periodicity in both x- and y-directions is assumed.

The distribution of uninterrupted segment lengths provides a measure of the domain's tendency to support flow channeling and to modify turbulent structures for a given wind direction. Following Lu et al. [2023], the segment lengths are normalized by the mean building height, yielding the modified alignedness metric γ_m^*. This scaling reflects the fact that canopy geometry primarily influences turbulence within the RSL, whose height scales with the building canopy height [Inagaki et al., 2012].

The remaining problem is to contract the information into one number for each direction θ. Lu et al. [2023] use the maximum line-segment length of each line and then averaged over all the lines. We pursued a statistically more representative approach. After several numerical experiments with both generic and real building canopies, we ended up with the following concept: first, 99% of the shortest line segments in the distribution are abandoned, and average

length from the remaining 1%–the long-segment tail–is taken as γ at height z and in direction θ. Also lower cut-offs were tested, but they turned out to not yield a sufficiently sensitive metric for alignedness. The gamma-computation is repeated at several heights up to the mean building height in the domain, and finally $\gamma(z,\theta)$ is vertically averaged as

$$\gamma_m(\theta) = \frac{1}{\overline{h_b}} \int_0^{\overline{h_b}} \gamma(z,\theta) dz. \tag{1}$$

The purpose of this vertical averaging is to put more emphasis on deeper canyons than shallow ones as very shallow canyons supposedly have only weak effects on wind flow.

Terrain-height variations are not taken into account in γ although steep changes may influence the channelling tendency. In this work we assume relatively small and slow terrain-height variations. In this study, $\gamma_m(\theta)$ is computed with 2°-steps in θ for all cases.

The drawback of γ_m is that it does not only measure the importance of canyon-like structures in a given direction but it also measures the presence of less direction-dependent widely open areas. It can attain high values both in structures dominated by aligned canyons and in structures dominated by openings wide in all directions. Such structures supposedly have different effects on mean flow and turbulent structures and the latter kind of structures do not show much channeling potential. In order to distinguish such different structures from each other, we introduce a non-dimensional γ_m-variability parameter

$$\Delta\gamma_m^* = \frac{\max(\gamma_m(\theta)) - \min(\gamma_m(\theta))}{\max(\gamma_m(\theta))}, \qquad 0 \leq \Delta\gamma_m^* \leq 1, \tag{2}$$

where the maximum and minimum of $\gamma_m(\theta)$ is taken over the directions θ. If $\Delta\gamma_m^*$ shows large values, it is probably important to study the $\gamma_m(\theta)$-distribution and to identify possible peaks which may indicate dominance of canyon-like structures.

Figure 1 shows the topography and its $\gamma(\theta)$ for a small test area featuring almost rectangular layout with quite long street canyons roughly in directions 345° and 75°. The γ-distribution shows clear peaks in those directions as expected. Figure 2 shows another example from a somewhat larger urban area with more variable building layout than in first example shown in Fig. 1. Here γ_m gets higher values than in the first example and shows only one clear peak, but its variability is clearly lower $\Delta\gamma_m^* = 0.432$ indicating less organized alignment of canyons.

In summary, the nine chosen urban canopy parameters are:

- average height of the building canopy, $\overline{h_b}$
- standard deviation of h_b, σ_{h_b}
- plan-area fraction of the plant-canopy, λ_{pb}
- frontal-area fraction in the x-direction, λ_{fbx}
- frontal-area fraction in the y-direction, λ_{fby}
- minimum alignedness, $\min(\gamma_m(\theta))$
- maximum alignedness, $\max(\gamma_m(\theta))$
- average alignedness, $\overline{\gamma_m(\theta)}$
- alignedness variability, $\Delta\gamma_m^*$

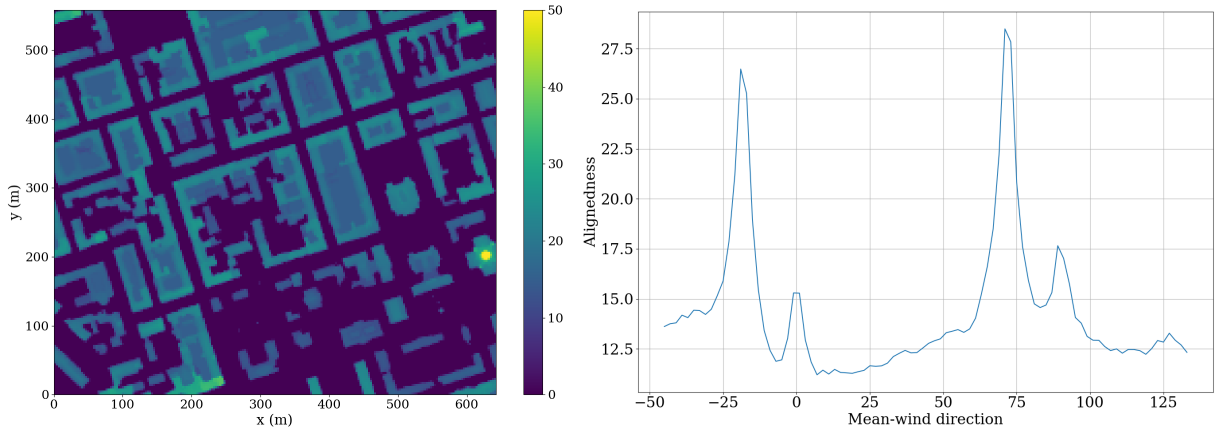


Figure 1: Building topography of a small urban test area with almost rectangular building layout with the colour indicating building height (left), and its $\gamma_m(\theta)$ distribution (right). Due to the symmetry, mean-wind direction θ is varied only from 315° to 135° via 0° (the directions from 315° to 0° are shown here as from −45° to 0°). Note the distinct γ_m-peaks around the dominant street canyon directions. This highly organized alignedness is also seen as a high value of $\Delta\gamma_m^* = 0.607$ although γ_m-values themselves are quite small in this case partially because the test domain is small.

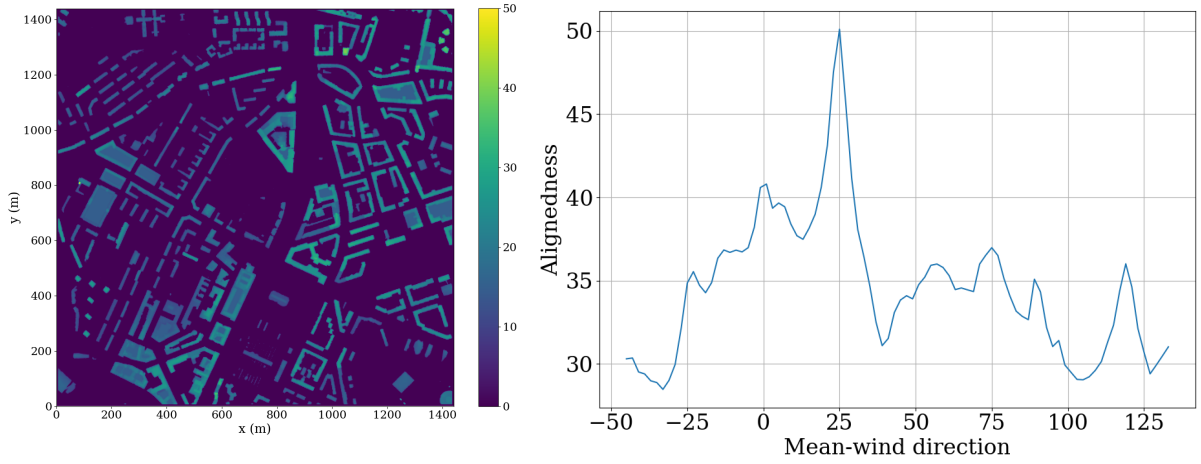


Figure 2: Building topography of a larger urban area with more variable building layout (left) than in first example shown in Fig. 1, and its $\gamma_m(\theta)$ distribution (right). Here γ_m gets higher values than in the first example and shows only one clear peak, but its variability is clearly lower $\Delta\gamma_m^* = 0.432$ indicating less organized alignment of canyons.

3.3 Set of plant canopy parameters

Like the building canopy, also the plant canopy–essentially trees–directly influence both mean flow and turbulence within the roughness sublayer. Therefore also trees have to be parameterized.

We chose to use the following five plant-canopy parameters:

- average product of h_p and estimated LAD, $\overline{h_p \times \mathrm{LAD}}$
- standard deviation of $h_p \times \mathrm{LAD}$, $\sigma_{h_p \mathrm{LAD}}$
- plan-area fraction of the plant-canopy, λ_{pp}
- frontal-area fraction in the x-direction, λ_{fpx}
- frontal-area fraction in the y-direction, λ_{fpy}

Here $h_p(x, y)$ is the plant-canopy height, LAD is the estimated leaf-area density ($\mathrm{m}^2/\mathrm{m}^3$). Unfortunately at the time of writing this report, we do not have detailed spatially varying LAD-information available. Instead, we simply use a constant value LAD $= 0.25\,\mathrm{m}^2/\mathrm{m}^3$ everywhere in all plant canopies in this study. If possible and feasible this will be refined in later stages of the work. Again, we only compute λ_{fp} in the x- and y-directions for the same reason as in case of λ_{fb}. In some cases λ_{fpx} and λ_{fpy} differ somewhat more from each other than λ_{fbx} and λ_{fby}. These differences occur mainly in those cases which are built from relatively small repeated patches leading to more organized patterns than the other cases, namely: G21, G22, G41 and G42 defined in the next section and in Tables 1 and 2 therein.

4 Suite of selected built environments

The suite of built-environment cases is designed to represent a range of urban configurations while keeping the total number of cases manageable. A key challenge in parameterizing built environments is the presence of domain-scale heterogeneities, which complicate their representation using a single set of parameters. In contrast, environments with primarily small-scale heterogeneity are generally more amenable to such parametrization. One of the central research questions is therefore to assess the error and uncertainty introduced when domain-scale heterogeneity is neglected and only smaller-scale variations are retained.

To address this, four real built environments of approximately $4\,\mathrm{km} \times 2\,\mathrm{km}$ are selected as reference cases for constructing domain-scale-homogenized configurations. Two of these correspond to peri-urban areas near potential SMR sites and exhibit strong large-scale heterogeneity, while the other two represent a suburban and a relatively homogeneous urban environment.

Generic cases are generated by extracting a representative subdomain (including buildings and vegetation) from each real environment and tiling it periodically to fill a domain of equal size. The terrain height field is retained from the corresponding real case; its variation is generally small. Some generic configurations are representative of the source area, while others reflect nearby residential areas potentially affected by plume dispersion. The suitability of these alternatives in cases with strong source–surrounding contrasts is an open research question.

Multiple generic cases are derived from each real environment. An example of a real and corresponding generic building layout is shown in Fig. 3. Fig. 3 left panel shows part of Sorsasalo, Kuopio (southern part) and Vuorela, Siilinjärvi (middle and northern parts). The right panel shows a generic case repetitively filled with a relatively small building pattern cut from Vuorela residential area. Corresponding vegetation rasters are created in the same way. The purpose of this procedure is to eliminate most of the large-scale heterogeneities from the building and vegetation patterns. The dispersion results for the real and corresponding generic cases will be compared at a later stage of the project to assess the impact of large-scale heterogeneities and

the feasibility of the parameterization in large-scale heterogeneous real cases. Note that not all larger-scale heterogeneity is removed, for example in this case the the highway number 5 passing through Vuorela and seen as a buildingless canyon in roughly south-north direction is purposedly left in the generic case because it is expected to have an important channeling tendency and thus strongly characterizing this case. It is more easily seen in the generic case. The real cases are described in Sec. 4.1, and the generic cases in Sec. 4.2.

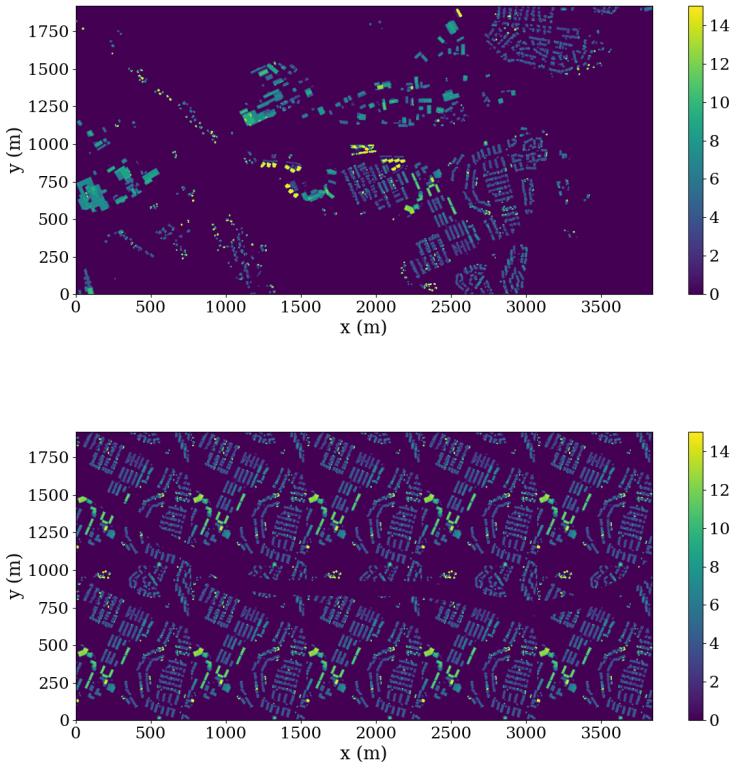


Figure 3: Examples of a real and corresponding generic domain-scale homogenized building topographies. North is to the right. The upper panel shows part of Sorsasalo, Kuopio (southern part) and Vuorela, Siilinjärvi (middle and northern parts). The lower panel shows a generic case filled with a building pattern cut from Vuorela residential area. The hazard scenario is that the release will occur in Sorsasalo industrial area near the southern edge of the domain and the plume will spread north to Vuorela residential area.

4.1 Real built environments

We selected four different kinds of real built environments as starting points to generate generic environments and to act as comparison references to the generic cases. They are introduced below. These four real built environments were chosen to this research since they either represented publicly known potential SMR sites or brought important area variation from dense building structures, scattered trees, to detached houses, apartment buildings and ware-house structures.

4.1.1 R1 Helsinki Vuosaari

Vuosaari port area is one of the potential SMR sites. Building and plant canopy maps are shown in Appendix A Figs. 4 and 5. Parameter values are listed in Tables 1 and 2. R1 represents a heterogeneous peri-urban domain combining a flat port area (east) and a residential area (west). The port consists of large, low-rise warehouses ($\sim 10\,\mathrm{m}$) with minimal plant canopy, while the residential area contains moderately sized apartment buildings ($\overline{h_b} \approx 9\,\mathrm{m}$) and relatively tall plant canopy ($\overline{h_p} \approx 16.4\,\mathrm{m}$), separated by open and semi-forested areas. The domain size in horizontal directions is $3840\,\mathrm{m} \times 1920\,\mathrm{m}$.

The case exhibits low to medium λ_{pb} and λ_{fb} due to extensive non-built areas. Mean alignedness is high ($\overline{\gamma_m} = 236\,\mathrm{m}$), but directional variability is weak ($\Delta\gamma_m^* = 0.242$), indicating domi-

nance of open areas rather than canyon structures. Plant canopy effects are significant overall despite their absence in the port. However, there are two cranes which are modelled as trees because their trussed construction is better modelled as porous media like trees rather than as solid obstacles. The hazard scenario assumes a release in the port area transported toward residential areas.

4.1.2 R2 Kuopio/Siilinjärvi Sorsasalo-Vuorela

Like Vuosaari port, Sorsasalo is also one of the potential SMR sites. Building and plant canopy maps are shown in Appendix A Figs. 6 and 7. Parameter values are listed in Tables 1 and 2. R2 combines an industrial release site in Sorsasalo with a residential and light-industrial area in Vuorela. The domain includes a major highway and the Siilinsalmi strait. The domain size in horizontal directions is 3840 m × 1920 m, the same as in R1.

Buildings are generally low ($\overline{h_b} \approx 5.5$ m), while plant canopy patches ($\overline{h_p} \approx 13.5$ m, $\lambda_{fp} \sim 0.25$) strongly influence flow. Alignedness is quite high ($\overline{\gamma_m} = 422$) with two peaks, one around 0° (the highway) and another around 45° (the strait), but directional dominance remains rather weak ($\Delta\gamma_m^* = 0.306$). Compared with R1, channeling is more associated with linear structures, while plant canopy effects are relatively stronger. The hazard scenario considers plume transport toward Vuorela.

4.1.3 R3 Helsinki Kallio-Hakaniemi-Kruununhaka

Building and plant canopy maps are shown in Appendix A Figs. 8 and 9. Parameter values are listed in Tables 1 and 2. R3 represents the most urban case, with high $\overline{h_b}$, λ_{pb}, and λ_{fb}, and relatively low plant canopy fractions. The modelling domain has been rotated 90° counterclockwise so that the real north is to the left unlike in cases R1 and R2. The horizontal domain size is (3840 m × 1728 m) which is slightly narrower in the y-direction than in the cases R1 and R2 (1920 m).

The domain contains dense building structures, scattered trees, and the Töölönlahti water body. Compared with R1–R2, it is more homogeneous, although building density increases toward the south. Alignedness is low and broadly distributed ($\Delta\gamma_m^* = 0.28$), reflecting complex multi-directional street patterns and water-body effects. Several hazard scenarios with different release locations relative to the building structure both horizontally and vertically will be modelled.

4.1.4 R4 Turku Kaerla

Building and plant canopy maps for the suburban residential area of Kaerla are shown in Appendix A Figs. 10 and 11. Parameter values are listed in Tables 1 and 2. R4 represents a suburban environment combining detached houses, apartment buildings, and warehouse-type structures with significant plant canopy coverage. The domain is not oriented in the north-south direction but it has been rotated counterclockwise by about 118°. The horizontal domain size is 3840 m × 1728 m i.e. the same as in R3.

λ_{pb} and λ_{fb} are low, and $\overline{\gamma_m}$ is quite low as well (152 m) with mild peaks in directions around 0°, 45° and 90° but low $\Delta\gamma_m^* = 0.280$ because of the quite large non-built areas with no clear directionality. Compared with R3, as $\overline{h_p} = 9$ m and $\lambda_{pp} = 0.385$ being very high, plant canopy effects are much stronger and may dominate flow characteristics. Several hazard scenarios with different release locations relative to the building structure both horizontally and vertically will be modelled.

4.2 Generic built environments

Generic cases are constructed by extracting representative subdomains from the real cases and tiling them to produce domain-scale homogeneous environments. The domain sizes are adopted from the corresponding real cases. Parameter values for all cases are given in Tables 1 and 2. Only case-specific features are described below.

4.2.1 G11 Generic homogenized Vuosaari-port-like warehouse area variant 1

A generic homogenized port environment (G11) was constructed to examine dispersion characteristics within a port setting (one of the potential SMR sites). As described in the R1 section, the original port area consists of several large, low-rise warehouses, a few taller industrial buildings, and extensive areas with smaller elements such as containers. In G11, only the principal warehouse and industrial buildings are retained, while smaller elements are excluded, resulting in a mildly sparsified configuration.

A base area of 820 m × 820 m is extracted and replicated in both x- and y-directions to generate a larger domain. To increase pattern diversity, each replicated tile is rotated by 90° relative to the previous one. From this periodic domain, an R1-sized region (3840 m × 1920 m) is selected such that the spatial position of the port buildings matches that of the original R1 configuration.

The mean building height is $\overline{h_b} = 11.0$ m, slightly higher than in R1, whereas R1 exhibits larger σ_{h_b} due to its more heterogeneous residential component. As shown in Table 1, λ_{pb} is higher than in R1 due to the absence of the low-density residential area and intervening open spaces, while λ_{fb} remains approximately unchanged.

The alignedness γ_m is lower than in R1 because large open areas are absent. In contrast, directional variability is significantly higher ($\Delta\gamma_m^* = 0.424$ vs. 0.242 in R1), indicating that γ_m is primarily governed by canyon-like structures rather than direction-independent areas. The case does not include plant canopy, and the terrain is completely flat.

4.2.2 G12 Generic homogenized Vuosaari-port-like warehouse area variant 2

G12 is an altered variant of G11 constructed to extend the parameter space. Compared with G11, all building heights are increased by 50%, increasing λ_{fb}, while a small number of buildings is removed to slightly decrease λ_{pb}.

These modifications affect γ_m in two opposing ways: removal of buildings increases absolute segment lengths, but normalization by $\overline{h_b}$ reduces them effectively by a factor of $\sim 2/3$, resulting in lower γ_m than in G11. As in G11, the case contains no plant canopy and the terrain is flat.

4.2.3 G13 Generic homogenized variant of Vuosaari residential area

Building and plant canopy layouts are shown in Figs. 14 and 15. G13 represents a homogenized residential counterpart of R1, created by duplicating the western half of the domain.

Compared with urban cases (G31, G32), building density is lower ($\lambda_{pb} = 0.134$ vs. 0.231 and 0.411), while plant canopy is much more dominant. Average plant canopy height is ~ 23 m and $\lambda_{pp} = 0.321$, several times larger than in urban cases. λ_{fb} is lower than in G31–G32 but higher than in R1.

Alignedness reflects both open areas at the duplication seam and major north–south streets, with a broad maximum at $-10° \leq \theta \leq 40°$ and $\Delta\gamma_m^* = 0.386$. Several release scenarios are considered, including one consistent with the R1 geometry.

4.2.4 G21 Generic homogenized variant of Vuorela, Siilinjärvi, residential area

In order to study the dispersion characteristics in a residential environment, we have created a generic homogenized variant based on the real neighbourhood of Vuorela, Siilinjärvi. Building

and plant canopy layouts are shown in Figs. 16 and 17. G21 is a homogenized residential environment derived from R2 by tiling a representative subdomain (1024 m × 768 m) to a full domain (1920 m × 3840 m), with a cleared corridor representing the highway.

Compared with R2, λ_{pb} and λ_{fb} increase significantly (by $\sim 2.5\times$ for λ_{pb}), while $\overline{\gamma_m} = 163$ is clearly lower due to the removal of large open regions. Directionality increases ($\Delta\gamma_m^* = 0.396$ vs. 0.306), reflecting repeated canyon structures.

The γ_m-distribution shows two broad peaks at $\theta \approx 0°-30°$, and at about 90°–130° (highway). Plant canopy characteristics remain similar to R2, though λ_{fp} increases and becomes the highest in the suite.

4.2.5 G22 Generic homogenized variant of Vuorela, Siilinjärvi, warehouse-area

For the case of a release in a warehouse type district, a generic homogenized variant was created by using the light-industry area of Vuorela, Siilinjärvi. Building and plant canopy layouts are shown in Figs. 18 and 19. G22 represents a homogenized industrial environment constructed from a smaller representative tile (256 m × 256 m), tiled to a full domain with a cleared highway corridor.

Compared with G21 and R2, buildings are more tightly spaced, yielding lower $\overline{\gamma_m} = 87.9$. However, directionality is strongest in the suite ($\Delta\gamma_m^* = 0.721$), partly due to low baseline γ_m values.

The distribution shows distinct peaks near $\theta \approx 0°$ and 90°. As in G21, repetition amplifies directional patterns. Plant canopy is sparse and highly fragmented, with reduced λ_{pp} and λ_{fp} and slightly lower $\overline{h_p \times \mathrm{LAD}}$ than in R2.

4.2.6 G31 Generic homogenized variant of Kallio, Helsinki

As mentioned in Sec. 4.1.3, the R3 domain shows somewhat different features in its northern half (left-hand half), and its middle and south parts (right-hand half). Therefore two homogenized generic variants are created first of them being homogenized variant of Kallio. Building and plant canopy layouts are shown in Figs. 20 and 21. As discussed in Sec. 4.1.3, G31 is constructed by duplicating the northern half of R3, excluding the Töölönlahti water body.

Compared with R3, mean building height is similar (16.6 m), while λ_{pb} is slightly lower and λ_{fb} unchanged. $\overline{\gamma_m}$ decreases (68.6 to 51.6) and $\Delta\gamma_m^*$ increases slightly (0.28 to 0.30), primarily due to removal of the water body.

Plant canopy parameters change only marginally, as vegetation is mainly located in the retained portion of the domain. Release scenarios follow those of R3.

4.2.7 G32 Generic homogenized variant of Kruununhaka/Kaisaniemi, Helsinki

Case G32 is constructed by tiling the rightmost quarter of R3, yielding a dense and highly uniform urban configuration. Building and plant canopy layouts are shown in Figs. 22 and 23.

This case has the highest $\overline{h_b} = 18.8$ m, $\lambda_{pb} = 0.411$, and λ_{fb} in the suite. γ_m is the lowest due to minimal open space, but directional variability is relatively high ($\Delta\gamma_m^* = 0.415$) due to aligned street canyons.

The γ_m-distribution exhibits multiple peaks (e.g. 343°, 41°, 71°, 89°, 131°) consistent with visible canyon orientations (Fig. 22). Plant canopy is sparse, reflected in low λ_{pp} and λ_{fp}.

4.2.8 G41 homogenized variant of Kaerla, Turku, detached-house area

Case G41 is constructed by tiling representative sub-areas from R4, producing a low-rise residential environment dominated by small detached houses. Building and plant canopy layouts are shown in Figs. 24 and 25.

Table 1: Summary of the urban-canopy parameters. Dimension of $\overline{h_b}$ and σ_{h_b} is m while other parameters are dimensionless.

Case	$\overline{h_b}$	σ_{h_b}	λ_{pb}	λ_{fbx}	λ_{fby}	$\min(\gamma_m)$	$\max(\gamma_m)$	$\overline{\gamma_m}$	$\Delta\gamma_m^*$
G11	11.0	3.60	0.248	0.048	0.050	92.3	160	127	0.424
G12	16.3	5.19	0.231	0.064	0.067	65.3	111	84.9	0.413
G13	9.18	6.29	0.134	0.083	0.082	108	176	135	0.386
G21	5.44	3.37	0.234	0.083	0.073	126	208	163	0.396
G22	6.62	3.00	0.255	0.070	0.077	55.0	197	87.9	0.721
G31	16.6	7.26	0.231	0.178	0.177	46.6	66.5	51.6	0.300
G32	18.8	7.05	0.411	0.230	0.241	23.7	40.6	32.6	0.415
G41	4.86	2.20	0.241	0.064	0.066	100	352	136	0.714
G42	11.4	7.29	0.235	0.121	0.124	51.3	111	70.7	0.537
R1	10.1	5.90	0.110	0.053	0.052	208	275	236	0.242
R2	6.30	3.87	0.092	0.033	0.032	364	525	422	0.306
R3	17.7	7.3	0.261	0.176	0.179	58.6	81.4	68.6	0.280
R4	7.22	4.86	0.212	0.064	0.065	134	186	152	0.280

Plant canopy is abundant ($\lambda_{pp} = 0.332$ vs. 0.385 in R4) and tall ($\overline{h_p} = 13.3\,\mathrm{m}$), greatly exceeding the mean building height (7.17 m). Accordingly, $\lambda_{pb} = 0.025$ only and $\lambda_{fb} \approx 0.03$ and flow dynamics are likely dominated by plant canopy effects.

Although $\lambda_{pb} = 0.224$ and alignedness indicates organized canyon structure, particularly in the dominant street direction, building effects are likely secondary to vegetation influences.

4.2.9 G42 homogenized variant of Kaerla, Turku, apartment-building area

Case G42 is constructed similarly to G41, but using a tile representing apartment-building areas from R4. Building and plant canopy layouts are shown in Figs. 26 and 27.

Compared with G41, buildings are taller and more influential ($\overline{h_b} = 8.74\,\mathrm{m}$ vs. 5.08 m in R4), while plant canopy ($\overline{h_p} = 9.24\,\mathrm{m}$) remains significant but no longer dominant. $\lambda_{pb} = 0.257$ and $\lambda_{fb} = 0.117$–0.134, both higher than in R4.

Alignedness is relatively strong ($\overline{\gamma_m} = 69.6$, $\Delta\gamma_m^* = 0.577$), with a dominant peak at $\theta = 90°$ due to seam-aligned canyons, and secondary peaks at 55° and 124°. Compared with R4, λ_{pp} decreases slightly while λ_{fp} increases due to the redistribution of vegetation structure.

4.3 Summary of the parameters

The UCP–values for each case described above are summarized in Table 1, and PCP-values in Table 2. The cases are selected such that they represent a variety of different kinds of built environments characterized by different features. For the first batch of LES runs in Task 1.2, four generic cases are selected such that each of them represent its own corner of the parameter space spanning large part of it. These cases are: G32, G41, G13 and G21. G32 is the most urban generic case with very little vegetation and strong channeling potential. G41 is more or less the opposite of G32 being dominated by trees taller than most of the buildings. G13 is a quite densely built suburban environment with relatively tall buildings but also with a lot of tall trees. G21 is somewhat like G41 but includes more large buildings than G41 and is expected to have stronger tendency to channeling. The rest of the generic cases are considered more intermediate in the paprameter space. Those as well as all the real cases are left to the next batches of LES runs to be performed in 2027.

Table 2: Summary of the plant-canopy parameters. All the plant-canopy parameters are dimensionless. Cases G11 and G12 do not feature trees at all.

Case	$\overline{h_p \times \mathrm{LAD}}$	$\sigma_{h_p\mathrm{LAD}}$	λ_{pp}	λ_{fpx}	λ_{fpy}
G11	0	0	0	0	0
G12	0	0	0	0	0
G13	4.08	1.44	0.321	0.309	0.296
G21	3.63	1.64	0.379	0.329	0.319
G22	2.71	1.49	0.163	0.150	0.140
G31	2.73	1.17	0.087	0.092	0.093
G32	2.99	1.26	0.040	0.042	0.044
G41	1.73	0.78	0.236	0.112	0.117
G42	2.56	1.02	0.379	0.165	0.163
R1	4.06	1.44	0.210	0.195	0.189
R2	3.37	1.67	0.394	0.262	0.249
R3	2.82	1.20	0.073	0.078	0.078
R4	2.21	0.96	0.374	0.127	0.127

5 Selected meteorological conditions

The LES simulations of dispersion for the cases described in Sec. 4 are performed for a representative set of meteorological parameters (MEPs). The most influential parameters are:

- mean wind speed $\overline{U}$
- wind direction θ
- surface-layer thermal stratification (hereafter referred to as stability)
- boundary-layer height z_t

From a dispersion perspective, low wind speeds are generally most relevant, as plume dilution scales with $\overline{U}$ such that higher wind speeds lead to lower concentrations and reduced deposition. Therefore, the analysis focuses on low to moderate wind speeds. Under neutral stability, results can be scaled to other wind speeds, whereas this scaling is not valid under non-neutral conditions.

Wind directions will be selected case by case in Task 1.2. For the real (R) cases, directions are chosen such that plumes are transported from the release location toward inhabited areas. For the generic (G) cases, directions are selected approximately along the longer horizontal dimension of the domain, with minor adjustments if needed.

Four stability conditions are considered, spanning from strongly convective boundary layer (CBL) via more weakly convective CBL and neutrally stratified boundary layer (NBL) to stably stratified boundary layer (SBL), corresponding to Pasquill classes B, C, D, and F, respectively. Class A is excluded as it occurs rarely in the Finnish climate and the stably stratified classes E and G are excluded to keep the amount of work manageable. The selected cases and corresponding external parameters are given in Table 3.

Stability depends on both the surface potential-temperature flux $F_{\theta S}$ and wind forcing: in convective conditions, increasing $F_{\theta S}$ enhances instability, while increasing wind speed reduces it. Stability is parameterized using the nondimensional parameter $-z_t/L$, where z_t is the boundary-layer depth (often denoted z_i in convective cases) and L is the Obukhov length,

$$L = -\frac{u_*^3}{\kappa\beta F_{\theta S}}, \tag{3}$$

where $u_* = (\tau_s/\rho)^{1/2}$ is the friction velocity, $\kappa \approx 0.4$ is the von Kármán constant, and $\beta = g/\theta_{\text{ref}}$ is the buoyancy parameter.

The parameter $-z_t/L$ is an internal quantity, as it depends on the simulated values of u_* and θ_{ref}, and is therefore determined *a posteriori* from the LES results. The only exception is neutral stratification, for which $F_{\theta S} = 0$ and thus $-z_t/L = 0$.

The computational setup is designed such that z_t remains approximately 600 m or lower in order to limit computational cost. For running the low-cost models, wind speed information at

Table 3: Selected meteorological conditions and parameters.

Description	z_t (m)	$\overline{U}(z_t)$ (m/s)	$F_{\theta S}$, (W/m^2)	Pasquill-class
CBL, weak wind	600	1-2	150	B
CBL, moderate wind	600	6-7	150	C
NBL, moderate wind	500	6-7	0	D
SBL, weak wind	200	1	-5	F

the boudary-layer top is not sufficient. It is needed at some height in the logarithmic layer and this depends on the case through different surface drag owing to different mean roughness in the cases. As LES-results for all the cases in the first batch (G32, G41, G13 and G21), lower-level wind speeds are estimated using our previous results from another project for the cases R3 and R4. Here it is assumed that R3 is sufficiently similar to G32 and G13 and R4 to G41 and G21. Naturally this assumption creates some uncertainty. This uncertainty will be assessed as soon as all the new LES-runs are completed. Wind speed is estimated to the height $z = [100]m$ and given in Table 4. These wind-speed estimates can further be transferred to lower height above the canopy layer by using the Monin-Obukhov similarity theory.

Table 4: Mean wind speed (m/s) estimated to the height $z = 100$ m.

Case	G32	G13	G41	G21
CBL, weak wind	0.6	0.6	1.1	1.1
CBL, moderate wind	5.2	5.2	5.8	5.8
NBL, moderate wind	4.5	4.5	4.8	4.8
SBL, weak wind	0.75	0.75	0.8	0.8

6 Next steps

The next step is to prepare the full set of input definitions required for LES simulations of the selected first batch of LES runs (see Sec. 4.3) in Task 1.2 followed by the execution of the simulations. The building and tree rasters presented here form part of the input dataset. In addition, a large number of boundary conditions, numerical-method control parameters, release definitions, and other model parameters must be specified. This phase, and particularly the LES simulations themselves, is computationally demanding.

We have prior experience in setting up, running, and analysing similar simulations. Preliminary LES simulations have already been conducted for cases R3 and R4, but these will be repeated using an extended set of release scenarios. In each case, multiple releases will be simulated with varying release heights and, in some cases, different horizontal locations. These activities fall under Tasks T1.2 and T1.4 of Work Package 1 (WP1).

In Work Package 2 (WP2), the LES results will be used to derive a reduced-order parametric description of wind statistics that captures the essential features of flow variability, turbulence, and dispersion in built environments. This development is based on the UCP and PCP

parametrization introduced in this report. The ultimate goal is to improve Gaussian-plume, Gaussian-puff, and Lagrangian dispersion models by making them more responsive to the characteristics of built environments.

7 References

References

M. Auvinen, S. Boi, A. Hellsten, T. Tanhuanpää, and L. Järvi. Study of realistic urban boundary layer turbulence with high-resolution large-eddy simulation. *Atmosphere*, 11(2), 2020. ISSN 2073-4433. doi: 10.3390/atmos11020201. URL `https://www.mdpi.com/2073-4433/11/2/201`.

City of Helsinki. Helsinki 3D. http://hel.fi/3D, 2015. Downloaded June 6th, 2026.

City of Turku. Turku region map service, open data, 3D-laserscanning datasets LAZ. http://turku.asiointi.fi/ims/, 2021. Downloaded June 6th, 2026.

Finnish Forest Centre. Paikkatietoaineistot, latvusmallit. https://www.metsakeskus.fi/fi/avoin-metsa-ja-luontotieto/aineistot-paikkatieto-ohjelmille/paikkatietoaineistot, 2026. In Finnish only. Downloaded June 1st, 2026.

A. Inagaki, M.C.L. Castillo, Y. Yamashita, M. Kanda, and H. Takimoto. Large-eddy simulation of coherent flow structures within a cubical canopy. *Boundary-Layer Meteorology*, 142:207–222, 2012.

J. Lu, N. Nazarian, M.A. Hart, E.S. Krayenhoff, and A. Martilli. Novel geometric parameters for assessing flow over realistic versus idealized urban arrays. *Journal of Advances in Modeling Earth Systems*, 15(7):e2022MS003287, 2023. doi: https://doi.org/10.1029/2022MS003287. URL `https://agupubs.onlinelibrary.wiley.com/doi/abs/10.1029/2022MS003287`. e2022MS003287 2022MS003287.

B. Maronga, M. Gryschka, R. Heinze, F. Hoffmann, F. Kanani-Sühring, M. Keck, K. Ketelsen, M.O. Letzel, M. Sühring, and S. Raasch. The parallelized large-eddy simulation model (palm) version 4.0 for atmospheric and oceanic flows: model formulation, recent developments, and future perspectives. *Geoscientific Model Development*, 8:1539–1637, 2015.

B. Maronga, S. Banzhaf, C. Burmeister, T. Esch, R. Forkel, D. Fröhlich, V. Fuka, K. F. Gehrke, J. Geletič, S. Giersch, T. Gronemeier, G. Groß, W. Heldens, A. Hellsten, F. Hoffmann, A. Inagaki, E. Kadasch, F. Kanani-Sühring, K. Ketelsen, B. A. Khan, C. Knigge, H. Knoop, P. Krč, M. Kurppa, H. Maamari, A. Matzarakis, M. Mauder, M. Pallasch, D. Pavlik, J. Pfafferott, J. Resler, S. Rissmann, E. Russo, M. Salim, M. Schrempf, J. Schwenkel, G. Seckmeyer, S. Schubert, M. Sühring, R. von Tils, L. Vollmer, S. Ward, B. Witha, H. Wurps, J. Zeidler, and S. Raasch. Overview of the palm model system 6.0. *Geoscientific Model Development*, 13(3):1335–1372, 2020. doi: 10.5194/gmd-13-1335-2020. URL `https://gmd.copernicus.org/articles/13/1335/2020/`.

National Land Survey. Elevation model 2 m. https://www.maanmittauslaitos.fi/en/maps-and-spatial-data/datasets-and-interfaces/product-descriptions/elevation-model-2-m, 2026a. Downloaded June 6th, 2026.

National Land Survey. Topographic database. https://asiointi.maanmittauslaitos.fi/-karttapaikka/tiedostopalvelu/maastotietokanta?lang=en, 2026b. Downloaded June 6th, 2026.

T.R. Oke, G. Mills, A. Christen, and J.A. Voogt. *Urban Climates*. Cambridge University Press, 2017.

A Building- and tree-height raster plots

A.1 Case R1 Helsinki Vuosaari

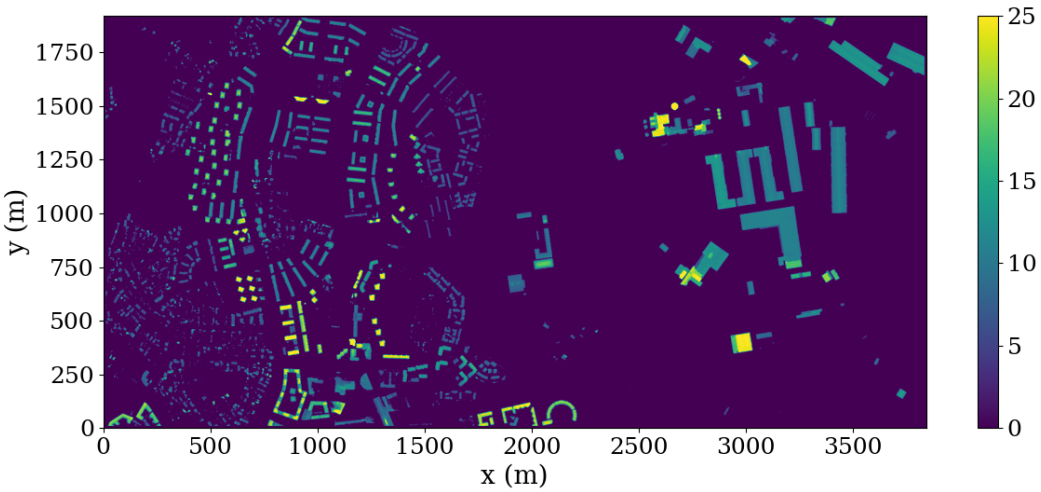


Figure 4: Building-height map of the case R1 Helsinki Vuosaari.

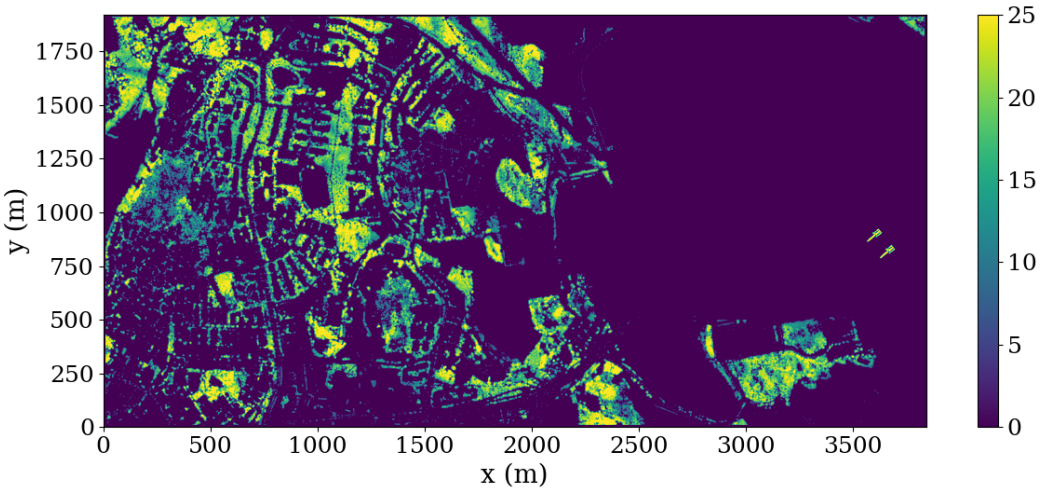


Figure 5: Tree-height map of the case R1 Helsinki Vuosaari.

A.2 Case R2 Kuopio/Siilinjärvi Sorsasalo-Vuorela

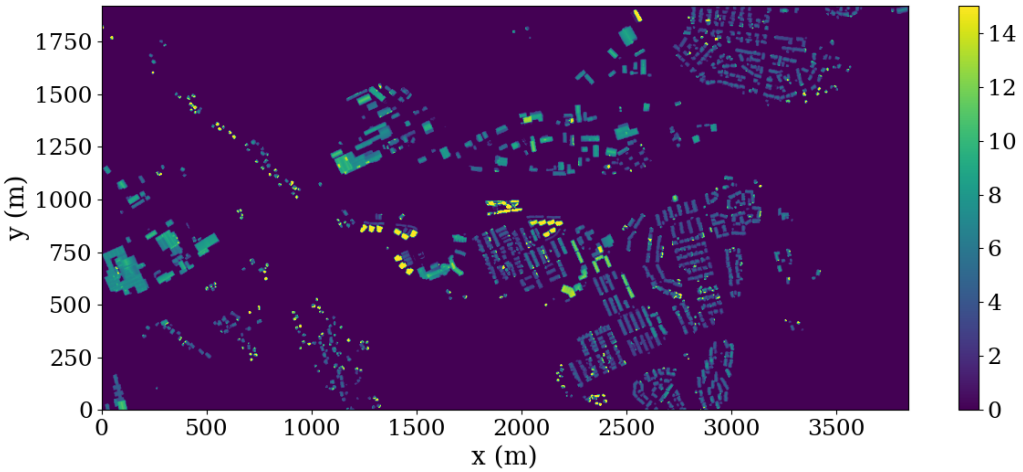


Figure 6: Building-height map of the case R2 Kuopio/Siilinjärvi Sorsasalo-Vuorela. Note that in this case north is to the right.

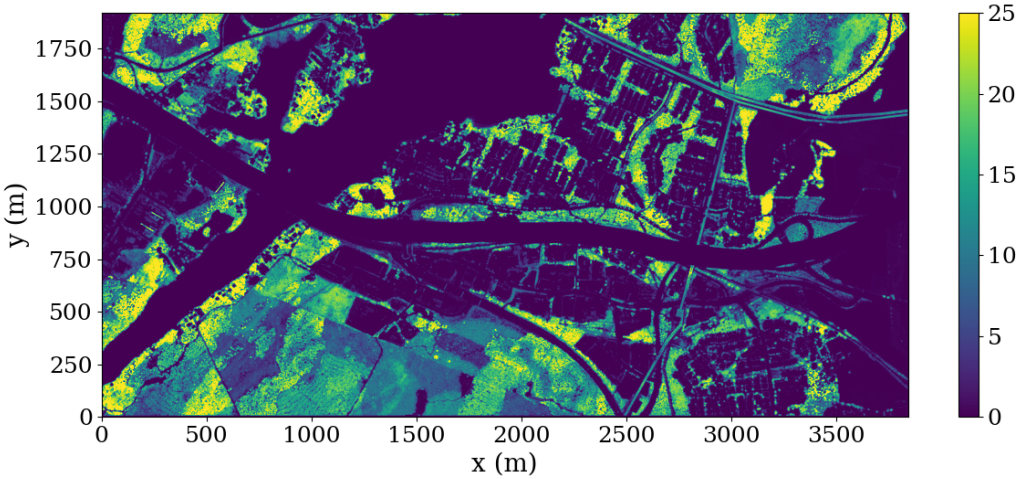


Figure 7: Tree-height map of the case R2 Kuopio/Siilinjärvi Sorsasalo-Vuorela. Note that in this case north is to the right. Note also the different colorscales.

A.3 Case R3 Helsinki Kallio-Hakaniemi-Kruununhaka

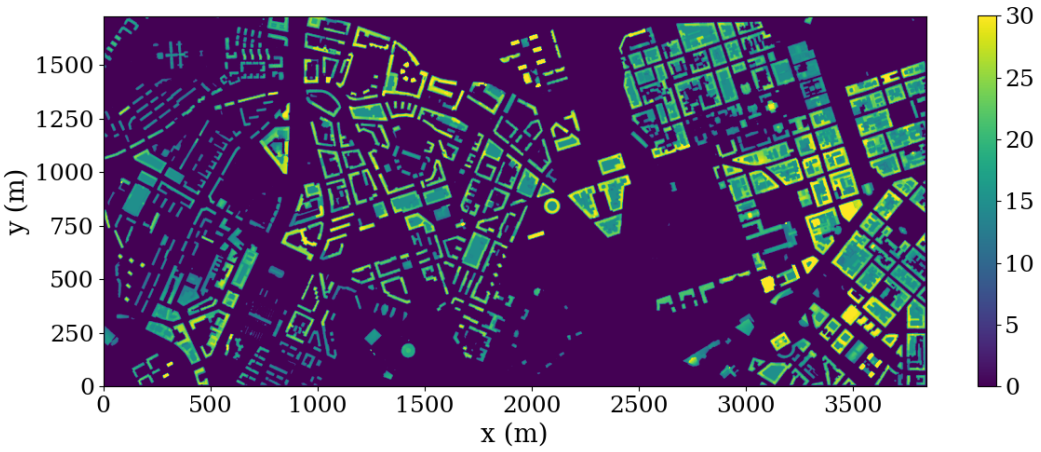


Figure 8: Building-height map of the case R3 Helsinki Kallio-Hakaniemi-Kruununhaka. Note that in this case north is to the left.

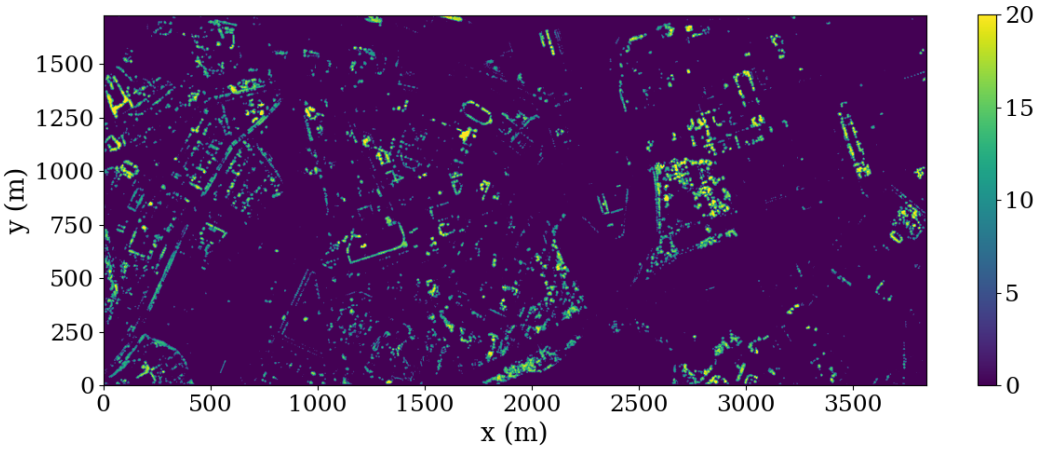


Figure 9: Tree-height map of the case R3 Helsinki Kallio-Hakaniemi-Kruununhaka. Note that in this case north is to the left. Note also the different colorscale.

A.4 Case R4 Turku Kaerla

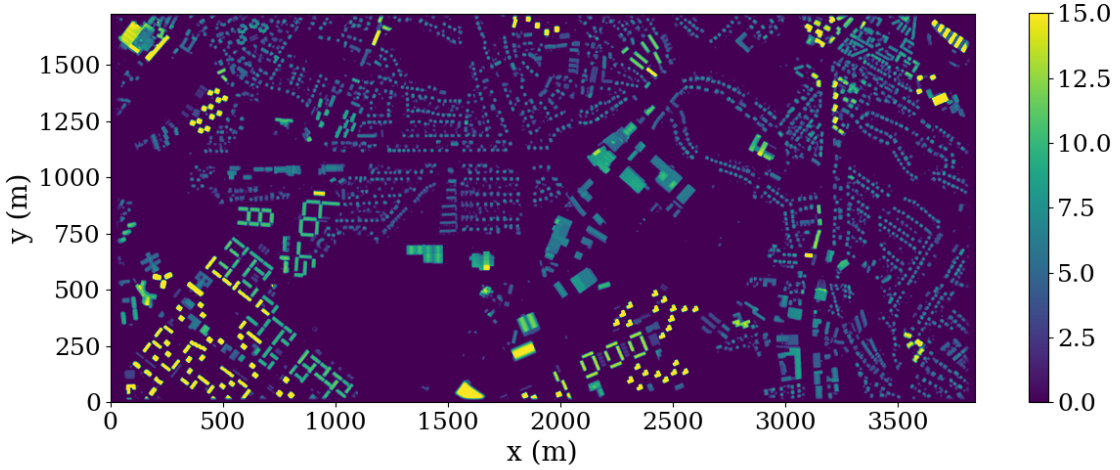


Figure 10: Building-height map of the case R4 Turku Kaerla. Note that this case is rotated 118° counterclockwise.

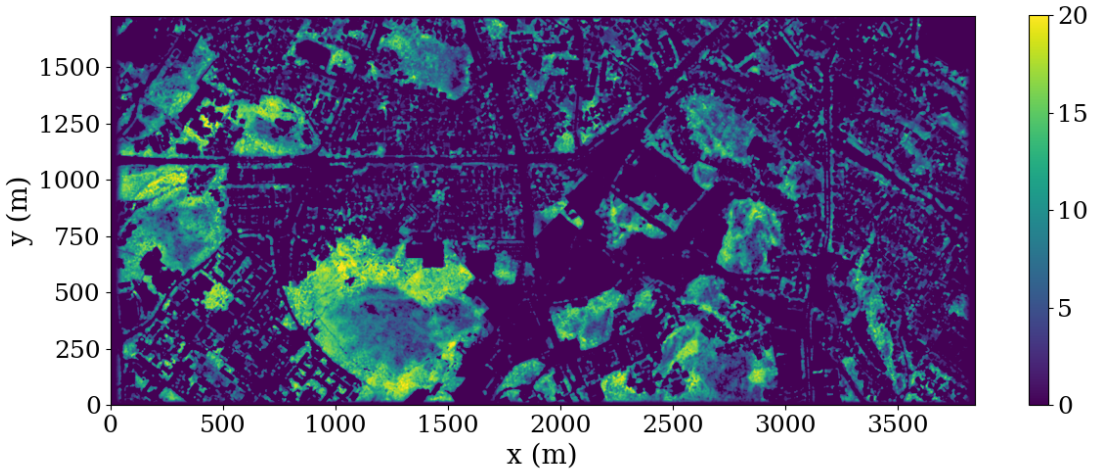


Figure 11: Tree-height map of the case R4 Turku Kaerla. Note that this case is rotated 118° counterclockwise. Note also the different colorscale.

A.5 Case G11 Generic homogenized Vuosaari-port-like warehouse area variant 1

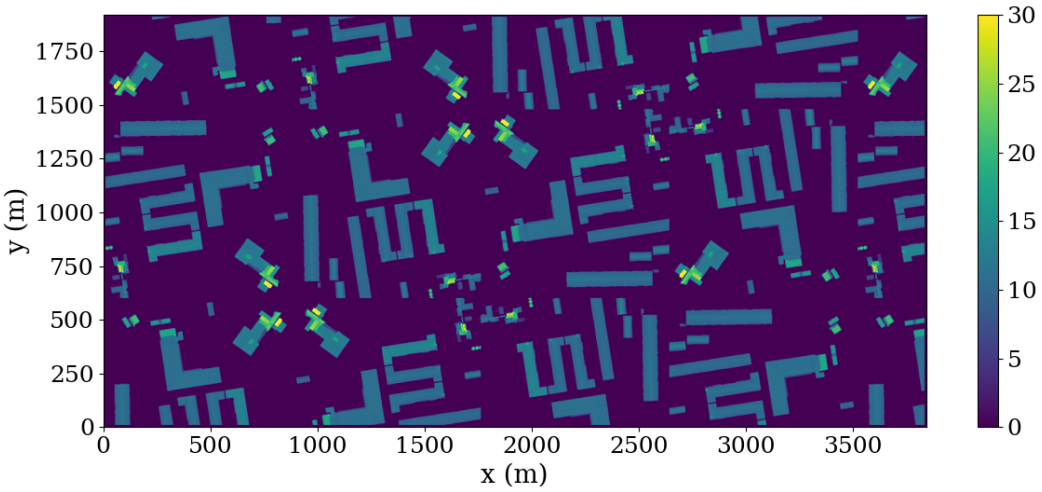


Figure 12: Building-height map of the case G11. There are no trees at all in this case.

A.6 Case G12 Generic homogenized Vuosaari-port-like warehouse area variant 2

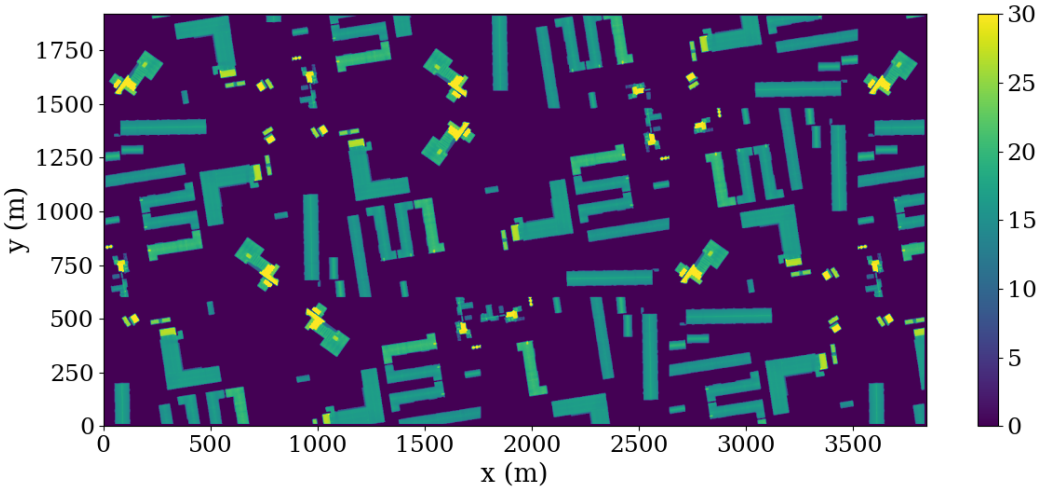


Figure 13: Building-height map of the case G12. There are no trees at all in this case. The colorscale is the same as for G11 for easier comparison.

A.7 Case G13 Generic homogenized variant of Vuosaari residential area

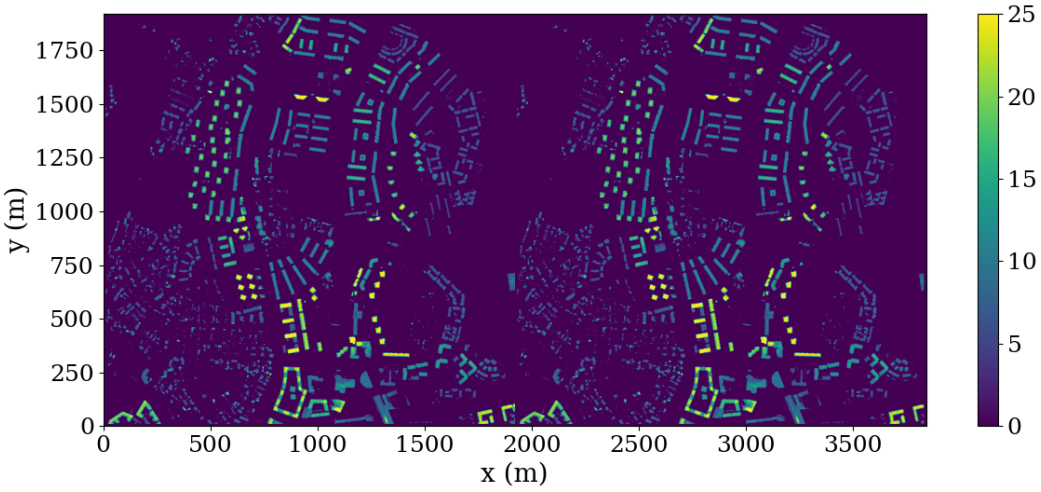


Figure 14: Building-height map of the case G13 homogenized variant of Vuosaari residential area.

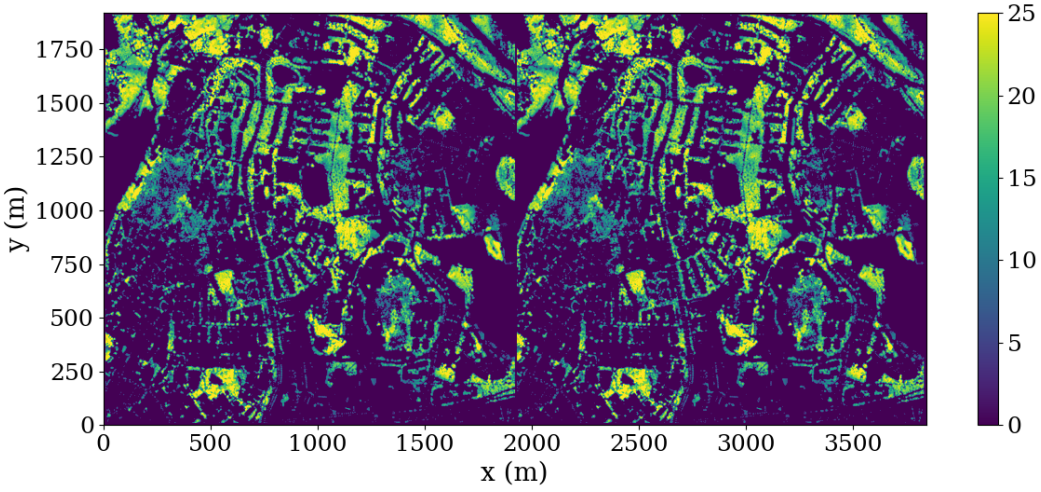


Figure 15: Tree-height map of the case G13 homogenized variant of Vuosaari residential area.

A.8 Case G21 Generic homogenized variant of Vuorela, Siilinjärvi, residential area

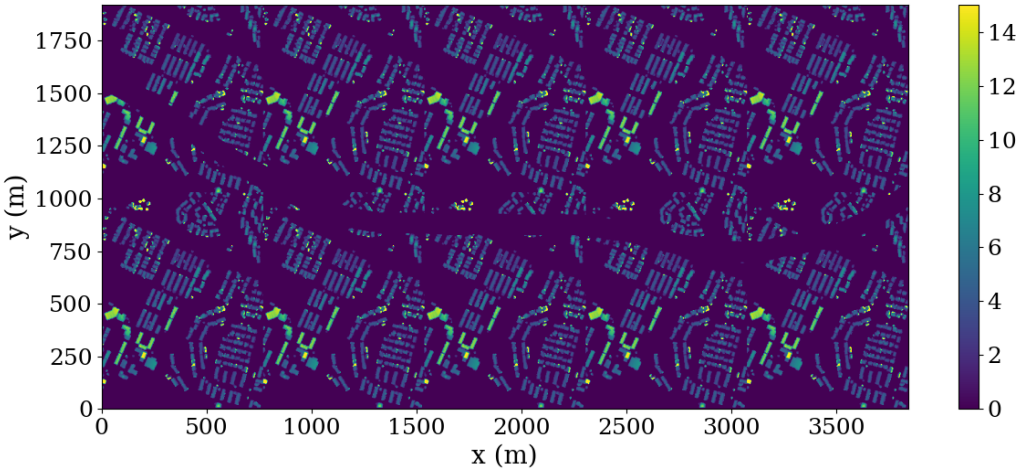


Figure 16: Building-height map of the case G21 homogenized variant of Vuorela, residential area.

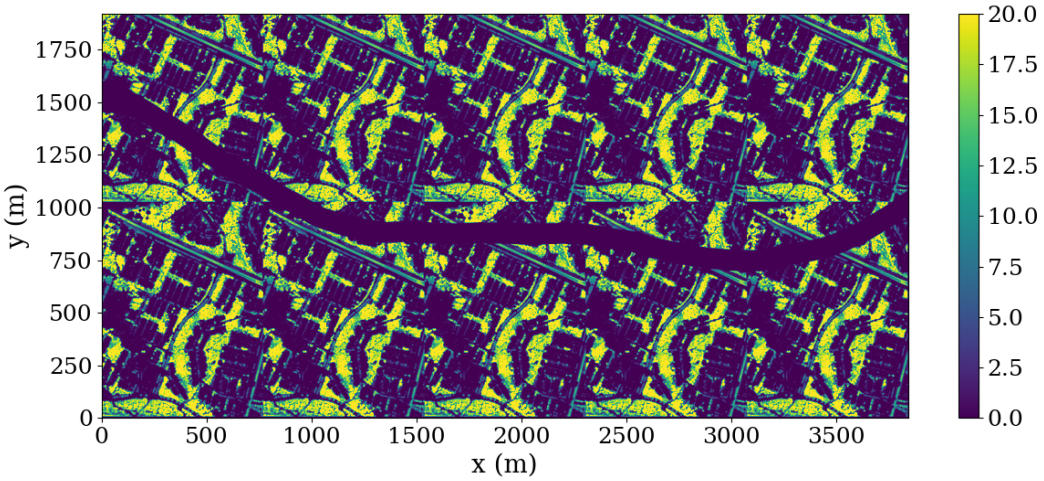


Figure 17: Building-height map (left) and tree-height map (right) of the case G21 homogenized variant of Vuorela, residential area. Note the different colorscales.

A.9 Case G22 Generic homogenized variant of Vuorela, Siilinjärvi, warehouse area

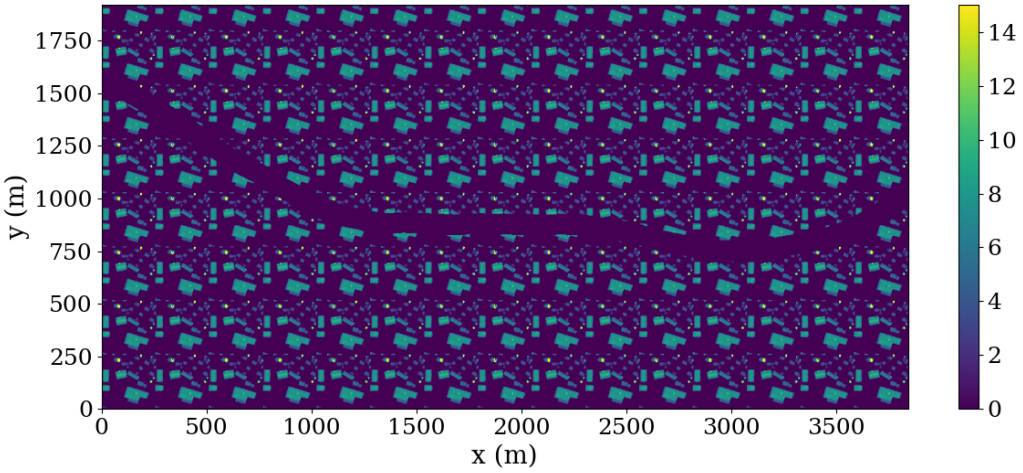


Figure 18: Building-height map (left) and tree-height map (right) of the case G22 homogenized variant of Vuorela, warehouse area.

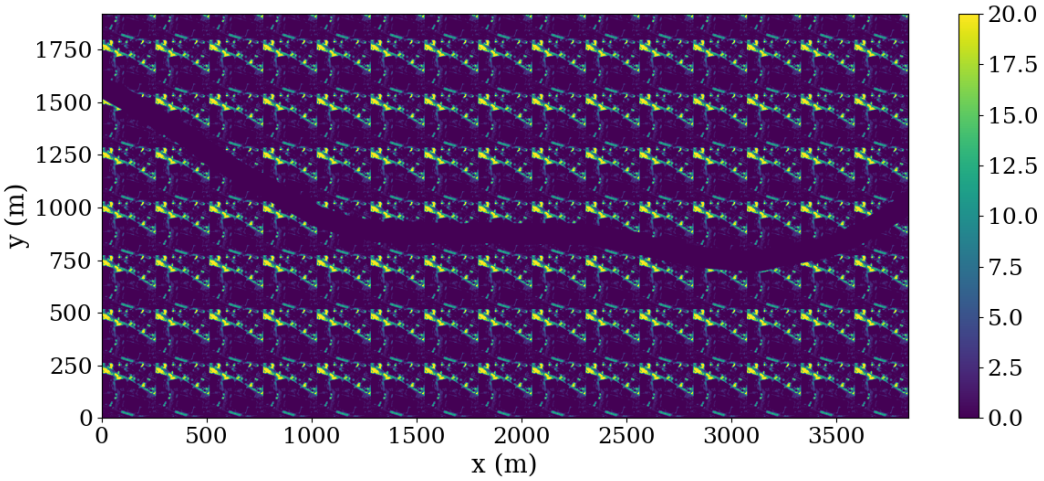


Figure 19: Building-height map (left) and tree-height map (right) of the case G22 homogenized variant of Vuorela, warehouse area. Note the different colorscales.

A.10 Case G31 Generic homogenized variant of Kallio, Helsinki

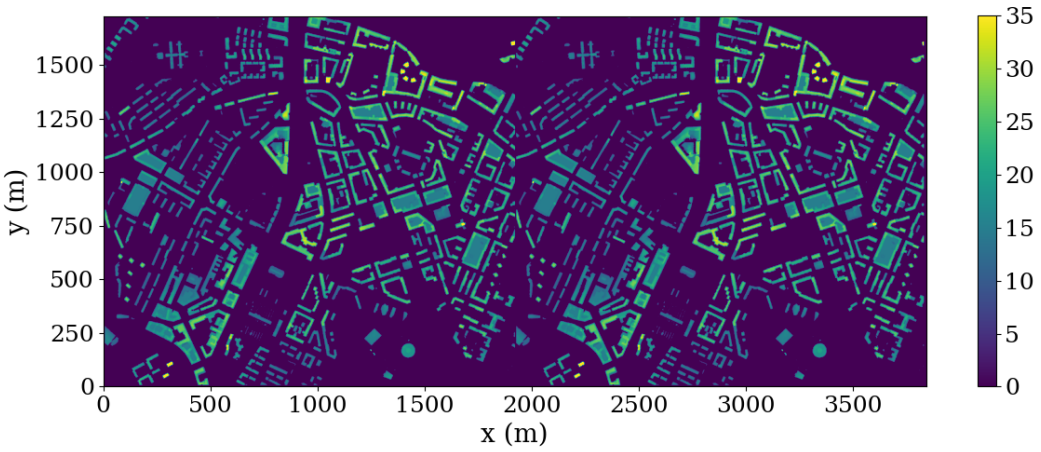


Figure 20: Building-height map of the case G31 homogenized variant of Kallio.

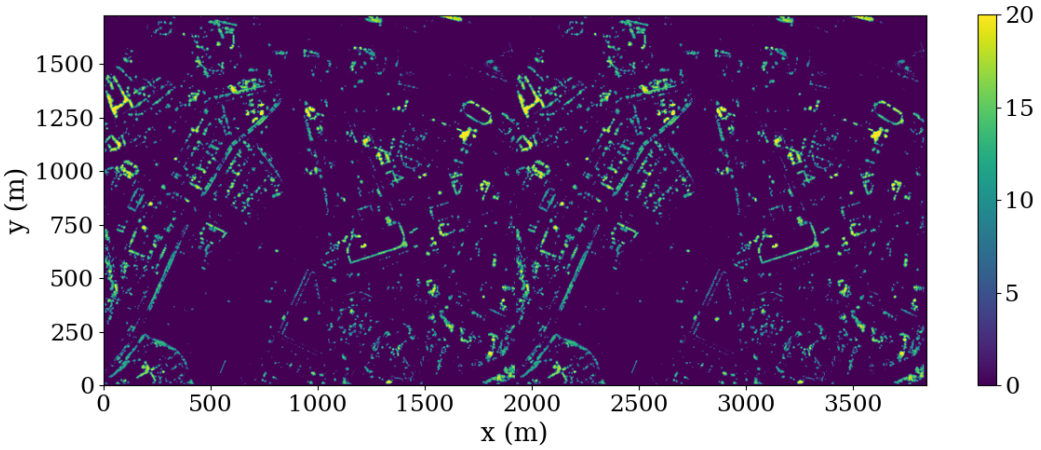


Figure 21: Tree-height map of the case G31 homogenized variant of Kallio. Note the different colorscale.

A.11 Case G32 Generic homogenized variant of Kruununhaka/Kaisaniemi, Helsinki

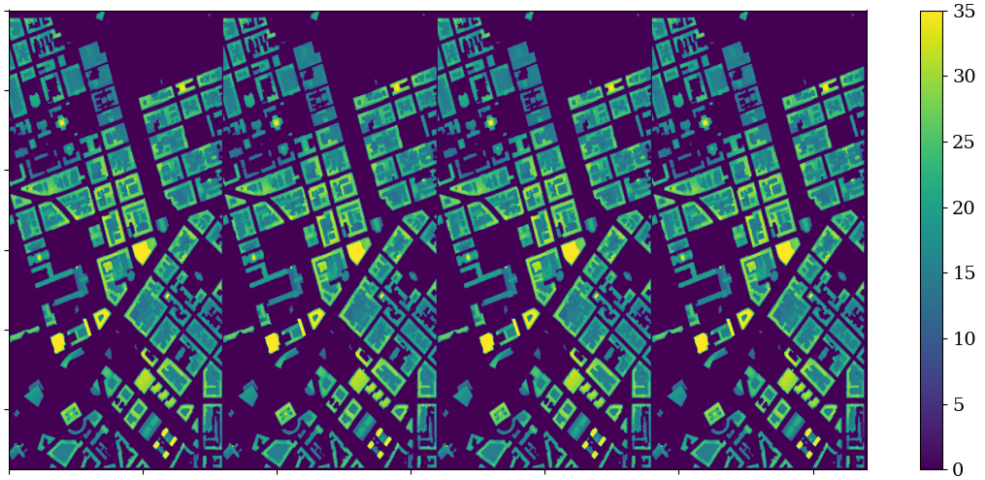


Figure 22: Building-height map of the case G31 homogenized variant of Kruununhaka/Kaisaniemi area.

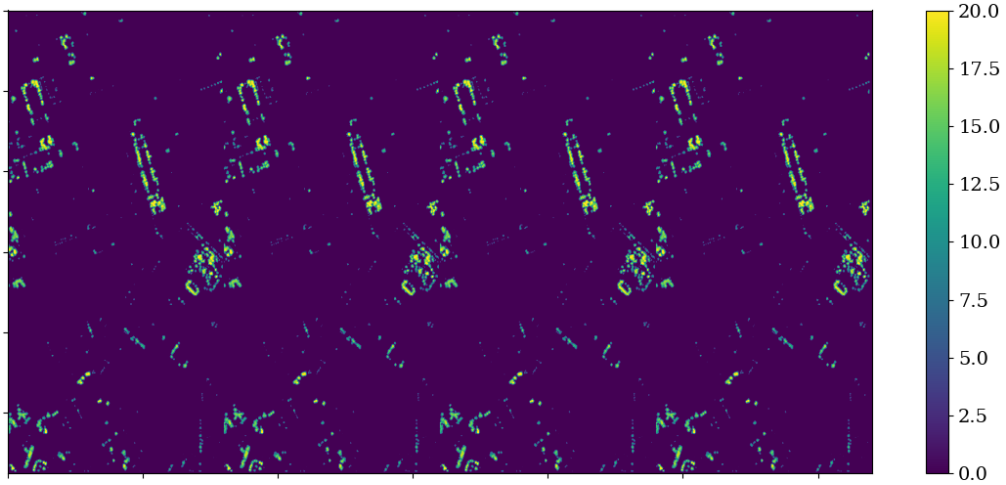


Figure 23: Tree-height map of the case G31 homogenized variant of Kruununhaka/Kaisaniemi area. Note the different colorscale.

A.12 Case G41 Generic homogenized variant of Kaerla, Turku, detached-house area

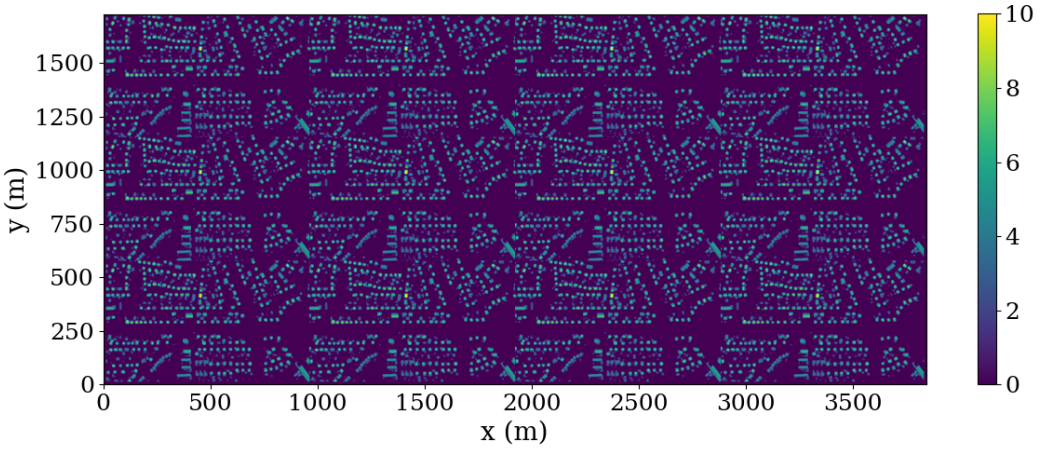


Figure 24: Building-height map of the case G41 homogenized variant of Kaerla, detached-house area.

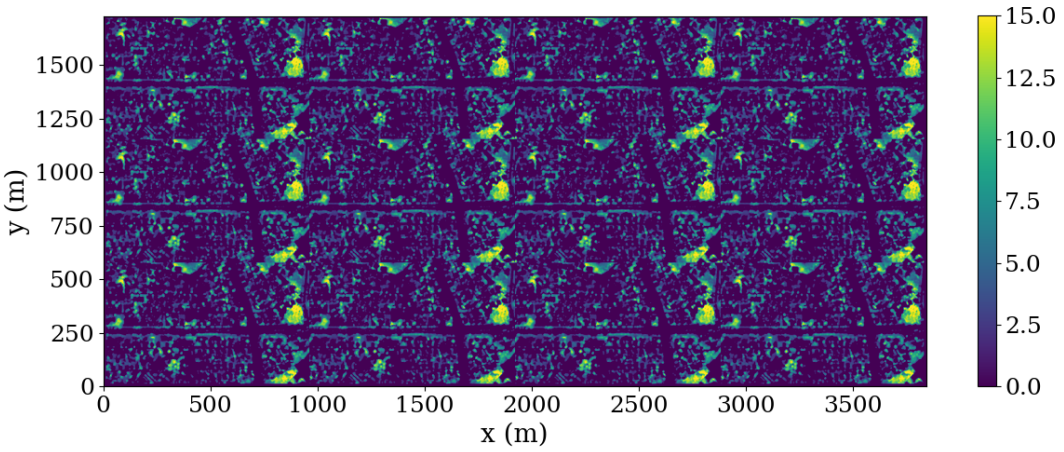


Figure 25: Tree-height map of the case G41 homogenized variant of Kaerla, detached-house area. Note the different colorscales.

A.13 Case G42 Generic homogenized variant of Kaerla, Turku, apartment-building area

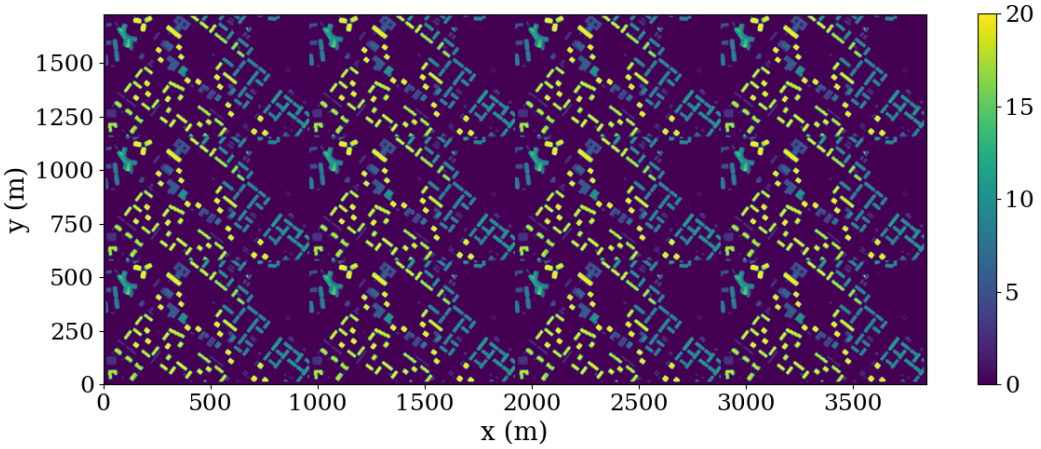


Figure 26: Building-height map of the case G42 homogenized variant of Kaerla, apartment-building area.

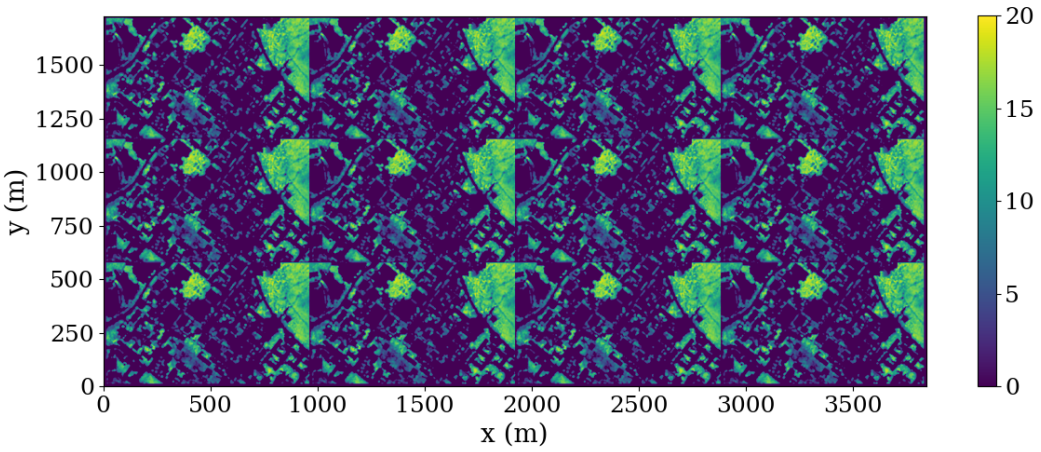


Figure 27: Tree-height map of the case G42 homogenized variant of Kaerla, apartment-building area.